

See discussions, stats, and author profiles for this publication at: <https://www.researchgate.net/publication/228113523>

Synthesis of MoS₂-C One-Dimensional Nanostructures with Improved Lithium Storage Properties

ARTICLE in ACS APPLIED MATERIALS & INTERFACES · JULY 2012

Impact Factor: 6.72 · DOI: 10.1021/am301055z · Source: PubMed

CITATIONS

76

READS

70

4 AUTHORS, INCLUDING:



Chaofeng Zhang
Hefei University of Technology

34 PUBLICATIONS 835 CITATIONS

[SEE PROFILE](#)



Zhiyu Wang
Dalian University of Technology

53 PUBLICATIONS 3,262 CITATIONS

[SEE PROFILE](#)



Zaiping Guo
University of Wollongong

236 PUBLICATIONS 5,818 CITATIONS

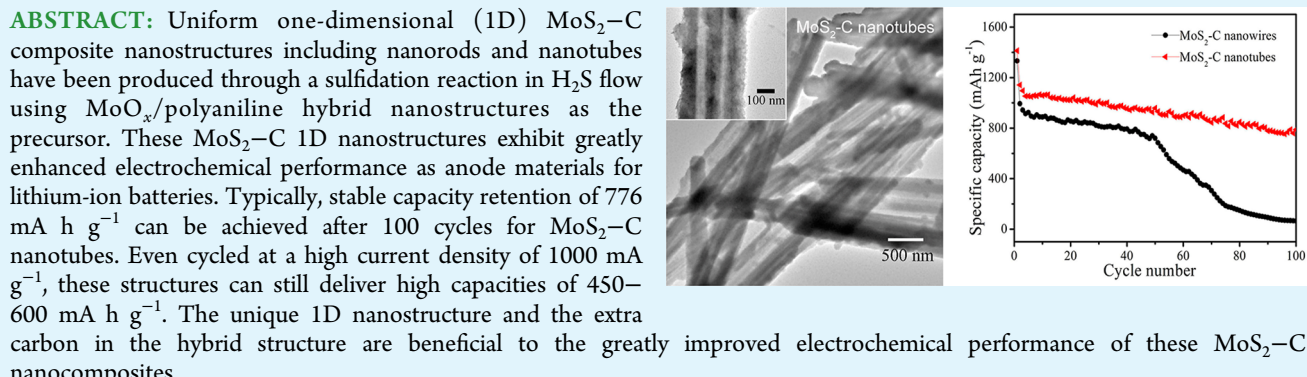
[SEE PROFILE](#)

Synthesis of MoS₂–C One-Dimensional Nanostructures with Improved Lithium Storage Properties

Chaofeng Zhang,^{†,‡} Zhiyu Wang,[‡] Zaiping Guo,^{*,†,§} and Xiong Wen (David) Lou^{*,‡}

[†]Institute for Superconducting & Electronic Materials and [§]School of Mechanical, Materials & Mechatronics Engineering, University of Wollongong, NSW 2522, Australia

[‡]School of Chemical and Biomedical Engineering, Nanyang Technological University, 70 Nanyang Drive, Singapore, 637457, Singapore



KEYWORDS: MoS₂, anode, lithium-ion batteries, hybrid structure, nanotubes, nanocomposites

INTRODUCTION

In recent years, rechargeable lithium-ion batteries (LIBs) have emerged as the most attractive power source in portable electric devices, and hybrid electric vehicles (HEVs) or electric vehicles (EVs).¹ Graphite is currently employed as the standard anode material for LIBs. However, its application in high-energy LIBs is largely hampered by the relatively low theoretical capacity (372 mA h g⁻¹) and the safety concern. To address the requirements in energy and power densities, safety, and cycling stability, further investigations have been conducted to develop new electrode materials.^{1,2} Recently, metal sulfides, such as, SnS₂, WS₂, CoS₂, FeS₂, CuS_x, and MoS₂, were extensively investigated as anode materials because of their high specific capacities and low cost.^{3–10} Among them, molybdenum disulfide (MoS₂) has received particular attentions because of its unique layered crystal structure which is beneficial for the intercalation of guest species, such as Li⁺,^{11–13} atoms and even large molecules.¹² As a result, various MoS₂ nanostructures, such as nanowires,¹⁴ nanosheets,^{7,15} nanoflakes,¹⁶ and nano-flowers,¹⁷ have been investigated as anode materials for LIBs. However, most of these MoS₂ based electrodes still suffer from fast capacity fading induced by intrinsically poor electrical/ionic conductivity and severe destruction upon repetitive lithium insertion.

One possible way to solve the capacity fading problem is to use hybrid nanostructures, where the active materials are embedded into the conductive matrix via chemical bonding or noncovalent forces. In such composites, in addition to all the desired functions of each constituent, strong synergistic effect

can be expected by integrating the individual components, hence realizing the full potential of the nanocomposite materials. In practice, the feasibility of this concept has been well demonstrated by several recent successes in synthesis of various MoS₂-based composite nanostructures. For example, layered MoS₂–graphene composites exhibit a high specific capacity of around 1100 mA h g⁻¹ with remarkable capacity retention while serving as anode materials for LIBs.¹¹ Uniform carbon-coated MoS₂ nanorods can manifest enhanced stability and reversibility upon extended cycling, compared with the bare MoS₂ nanorods without carbon coating.¹⁸ The graphene-like MoS₂–C also delivers high reversible capacity of 912 mA h g⁻¹ after 100 cycles.¹³ Evidently, the composite structure based on MoS₂ and carbonaceous matrix materials is highly promising as high-performance electrodes for LIBs. In this work, we report the rational design and mass production of MoS₂–carbon one-dimensional (1D) nanostructures (nanorods and nanotubes) by precisely controlled H₂S gas sulfidation of MoO_x/polyaniline (PANI) hybrid composites. When evaluated as potential anode materials for LIBs, these hybrid MoS₂–C 1D structures exhibit greatly improved electrochemical performance with excellent cycling stability and rate capability.

Received: June 12, 2012

Accepted: July 3, 2012

Published: July 3, 2012



EXPERIMENTAL SECTION

Materials Preparation. 1D nanostructures of MoO_x/PANI hybrid composite, including nanowires and nanotubes, were prepared according to a reported method with some modifications.¹⁹ First, $\text{Mo}_3\text{O}_{10}(\text{C}_6\text{H}_8\text{N})_2 \cdot 2\text{H}_2\text{O}$ was synthesized by dropwise adding appropriate amount of dilute HCl solution (1 M) into a 20 mL of mixture solution of ammonium heptamolybdate tetrahydrate (AHM, 1.24 g) and aniline (1.67 g) under stirring until the pH value reaches 4–5, followed by keeping at 50 °C for 8 h under stirring. The white precipitate of $\text{Mo}_3\text{O}_{10}(\text{C}_6\text{H}_8\text{N})_2 \cdot 2\text{H}_2\text{O}$ was collected by several rinse–centrifugation cycles and dried at 60 °C overnight. For the production of MoO_x/PANI hybrid nanowires, 0.335 g of as-prepared $\text{Mo}_3\text{O}_{10}(\text{C}_6\text{H}_8\text{N})_2 \cdot 2\text{H}_2\text{O}$ was ultrasonically dispersed in 20 mL of deionized water before 0.286 g of ammonium peroxydisulfate (APS) was added under stirring. Then an appropriate amount of dilute HCl solution (1 M) was added dropwise to adjust the pH value of the suspension to be around 2.0. The resultant suspension was kept under stirring at room temperature for another 10 h. The final product was collected by several rinse–centrifugation cycles before fully dried at 60 °C. A similar synthesis procedure can be employed to fabricate MoO_x/PANI hybrid nanotubes, whereas the pH value of the reaction system is adjusted to be around 3.0. For the preparation of 1D nanostructures of MoS_2-C composites, the MoO_x/PANI hybrid nanowires and nanotubes were annealed in H_2S atmosphere at 400 °C with a temperature ramp rate of 1 °C min⁻¹ for a certain period of time.

Materials Characterization. The samples were thoroughly characterized by field-emission scanning electron microscope (FESEM, JEOL, JSM-6340F), transmission electron microscope (TEM, JEOL, JEM-2010), powder X-ray diffraction (XRD, Bruker, D8-Advance X-ray Diffractometer, Cu K α radiation, $\lambda = 1.5406 \text{ \AA}$), nitrogen adsorption/desorption (Quantachrome Instruments, Auto-sorb AS-6B) and thermogravimetric analysis (TGA, Shimadzu, DRG-60).

Electrochemical Measurements. The electrochemical measurements were conducted using two-electrode Swagelok cells with pure lithium disk as the counter and reference electrode at room temperature. The working electrode consists of a test material (e.g., MoS_2-C nanowires or nanotubes), carbon black (Super-P-Li), and polyvinylidene difluoride (PVDF) in a weight ratio of 7:2:1. The electrolyte used is 1.0 M LiPF₆ in a 50:50 (w/w) mixture of ethylene carbonate and diethyl carbonate. Cell assembly is carried out in an Ar-filled glovebox with concentrations of moisture and oxygen below 1.0 ppm. The galvanostatic charge/discharge tests were performed using a Neware battery tester at different current densities with a cutoff voltage window of 0.01–3.0 V.

RESULTS AND DISCUSSION

The field-emission scanning electron microscope (FESEM) images of the MoO_x/PANI composite are shown in images A and B in Figure 1. A panoramic view reveals that the sample consists of uniform 1D nanostructures with a diameter of around 50–200 nm and a length of several micrometers. With this composite as the structure-directing precursor, 1D nanostructures of MoS_2-C composite can be obtained by the sulfidation of MoO_x/PANI in H_2S flow and simultaneous decomposition and partial carbonization of PANI at a relatively high temperature of 400 °C, as shown in images C and D in Figure 1. Despite the vast change in chemical composition, the as-obtained MoS_2-C products well retain the nanowire or nanotube morphology with slight variation in size. The formation of MoS_2-C 1D nanostructures is further evidenced by transmission electron microscope (TEM) observation. Both the MoS_2-C nanowires and nanotubes manifest well-defined and intact structures, as characterized by the TEM examination. The MoS_2-C nanowires (Figure 2A) have a diameter of 100–200 nm, whereas the nanotubes (Figure 2B) can be as thin as 50–150 nm with a wall thickness of 20–50 nm.

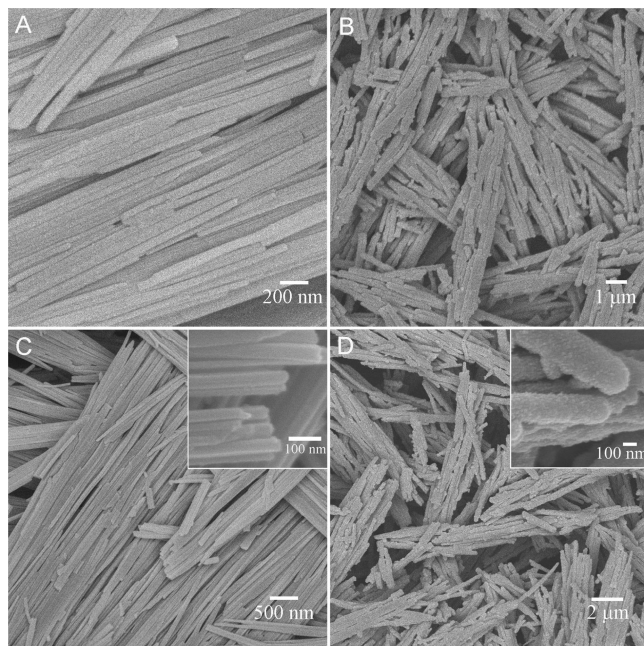


Figure 1. FESEM images of (A) MoO_x/PANI nanowires, (B) MoO_x/PANI nanotubes, (C) MoS_2-C nanowires, and (D) MoS_2-C nanotubes.

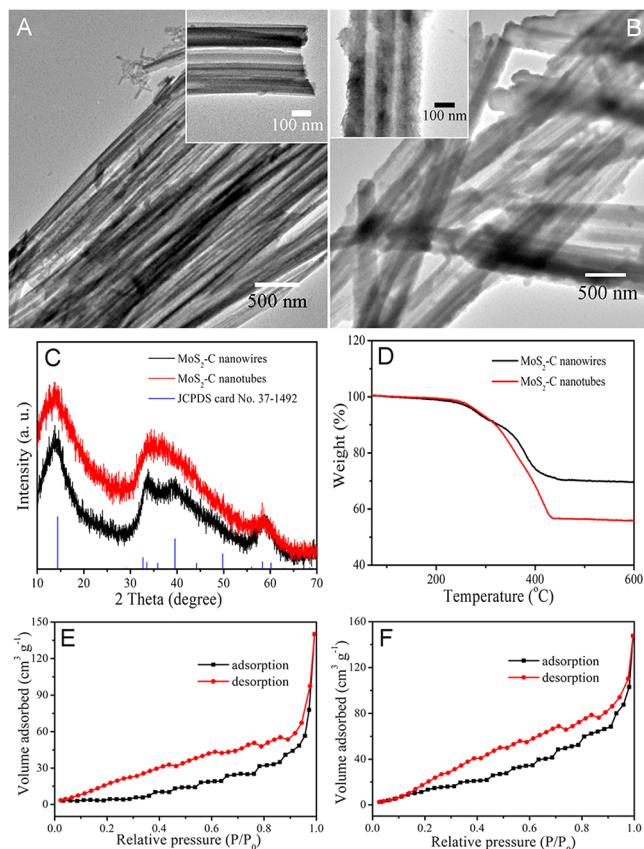


Figure 2. TEM images of (A) MoS_2-C nanowires and (B) MoS_2-C nanotubes. (C) XRD patterns of MoS_2-C nanowires and nanotubes, and lines from the standard card of MoS_2 . (D) TGA curves of MoS_2-C nanowires and nanotubes. The N_2 adsorption–desorption isotherms of the MoS_2-C (E) nanowires and (F) nanotubes.

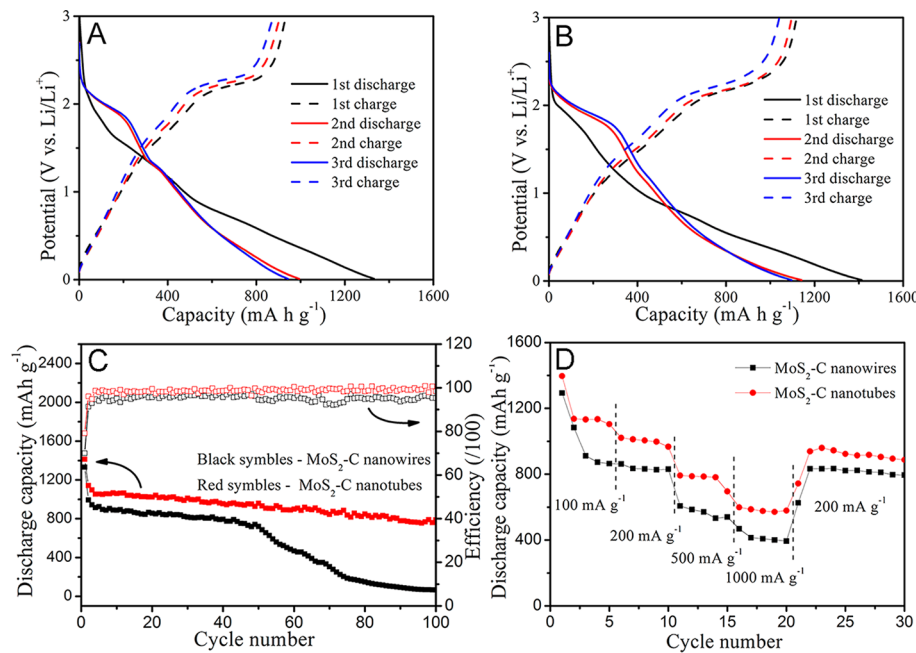


Figure 3. Discharge–charge voltage profiles for the first, second, and third cycles of (A) MoS₂–C nanowires and (B) MoS₂–C nanotubes. (C) Cycling performance and corresponding Coulombic efficiency for MoS₂–C nanowires and nanotubes at a current density of 200 mA g^{−1}. The tests are conducted between 0.01 – 3.0 V at a current density of 200 mA g^{−1}. (D) Rate behavior of the MoS₂–C nanowires and nanotubes at various current densities.

The crystallographic structure and phase purity of these MoS₂–C products are confirmed by X-ray powder diffraction (XRD), as shown in Figure 2C. All of the diffraction peaks can be assigned to hexagonal MoS₂ (JCPDS card no. 37–1492). Carbon is hardly identified within both samples due to their disordered amorphous nature. No signals from possible impurities such as MoO₃ and MoO₂ are detected. To determine the carbon content in the products, we conducted thermogravimetric analysis (TGA) of both MoS₂–C composites from room temperature to 600 °C in air flow with a ramp rate of 10 °C min^{−1}, as shown in Figure 2D. A common feature of both TGA curves is the large weight loss in the range of 250 – 450 °C, which is caused by the combustion of amorphous carbon and MoS₂ in air. The mass fraction of carbon in the MoS₂–C nanowires and nanotubes can be determined to be around 22% and 36%, respectively, assuming the complete conversion from MoS₂ to MoO₃. The N₂ sorption measurements (Figure 2E, F) show that the MoS₂–C nanotubes have much higher Brunauer–Emmett–Teller (BET) specific surface area of 81 m² g^{−1} than the MoS₂–C nanowires (14 m² g^{−1}). Apparently, this significant difference in surface characteristics can be attributed to the presence of hollow structure in the nanotubes.

In view of the great promise of MoS₂-based electrodes in LIBs, the electrochemical properties of the MoS₂–C 1D nanostructures are also investigated. Figure 3A shows the discharge–charge voltage profiles of the MoS₂–C nanowires for the first three cycles at a current density of 200 mA g^{−1} within a cutoff voltage window of 0.01–3.0 V. In agreement with previous reports,^{15,20} two poorly defined voltage plateaus at around 1.4 and 0.7 V are observed in the first discharge process, which are attributed to the insertion of Li⁺ ions into the interlayer space of MoS₂ and subsequent complete reduction of MoS₂ into Mo nanoparticles embedded in Li₂S matrix, respectively. The overall reaction during this process might be described as: MoS₂ + 4Li⁺ → Mo + 2Li₂S. In the

subsequent discharge process, two plateaus appear at around 1.9 and 1.2 V, while the plateau at about 0.7 V in the first discharge disappears. Upon the charging process, a plateau at about 2.2 V can be clearly identified for the first and subsequent cycles. Reasonably, the MoS₂–C nanotubes electrode displays similar electrochemical characteristics but a higher initial lithium storage capacity compared to the MoS₂–C nanowires electrode, as shown in Figure 3B. This can presumably be ascribed to the unique structural advantages of the tubular structure over the solid nanowires. More specifically, the presence of interior cavities inside the nanotubes offers substantially more interface with active sites to facilitate the storage of excess amount of lithium.^{21,22} Macroscopically, this contributes to the increased lithium storage capacity under identical testing conditions. Also for MoS₂–C nanotubes, the irreversible capacity loss in the first cycle is around 295 mA h g^{−1}, whereas MoS₂–C nanowires show a larger capacity loss of around 400 mA h g^{−1}.

The cycling performance of the MoS₂–C nanowires and nanotubes is shown in Figure 3C. The MoS₂–C nanowires exhibit a reversible discharge capacity of as high as 996 mA h g^{−1} in the second cycle at a current density of 200 mA g^{−1}, and stable capacity retention is observed for 50 cycles although the capacity drops rapidly after around 50 cycles to around only 65 mA h g^{−1} after 100 cycles. In contrast, the MoS₂–C nanotubes sample shows significantly improved cycling performance under the same conditions, as characterized by stable capacity retention of 776 mA h g^{−1} for the 100th cycle. This value is almost twice of the graphite-based materials (the theoretical capacity of graphite is ~372 mA h g^{−1}), and is superior to that of many MoS₂ based nanostructures such as carbon-coated MoS₂ nanorods,¹⁸ MoS₂ microspheres,¹⁵ MoS₂–CNT composite,⁷ and MoS₂ nanoflowers.¹⁷ For both MoS₂–C samples, high Coulombic efficiency of around 96–98% can be achieved despite that the lithium storage kinetics of MoS₂ is generally

sluggish. In addition to the cycling stability, the high-rate capability is also of great importance especially for high-power applications. Benefitted from the unique structures, these MoS₂–C composite materials exhibit excellent cycling response to continuously varying current rates although MoS₂ based electrodes are generally observed to suffer from sluggish kinetics. Even cycled at high rates of 1000 mA g⁻¹, discharge capacities of 450–600 mA h g⁻¹ can still be maintained, as shown in Figure 3D. After deep cycling at 1000 mA g⁻¹, a stable capacity of around 800–900 mA h g⁻¹ can be restored when the current density is reduced back to 200 mA g⁻¹. Among the two samples, again the MoS₂–C nanotubes sample exhibits slightly higher capacity at each current density. The better performance of MoS₂–C nanotubes may be attributed to their unique structural features. Specifically, the presence of hollow cavities provides effective buffering for the volume variation during Li⁺ insertion/extraction. The large surface area and extremely thin walls also endow the material with dramatic increment of reactive sites and electrode–electrolyte interface, as well as much shorter diffusion pathway, thus enabling efficient Li⁺/electron transport. Moreover, the higher carbon content in the MoS₂–C nanotubes further enhances the electronic conductivity and structural stability of the electrode. As a result, the MoS₂–C nanotubes reasonably show better cycling performance and rate capability than the nanowire counterpart.

The formation of the unique 1D composite nanostructures is beneficial to the improved electrochemical performance of MoS₂–C materials in this work. Specifically, the extremely reduced dimensions of MoS₂–C 1D nanostructures not only contribute to the improved electrode stability because of the reduced lattice strain associated with lithium intercalation, but also enhance the kinetics for Li⁺ and electron transport by shortening the diffusion pathway to nanoscale.²³ Moreover, the MoS₂–C 1D nanostructures, typically several micrometers in length, need only a few contact points to ensure efficient electron conduction, in contrast to the nanoparticle counterparts that may easily become electrically isolated as they expand and contract during charge–discharge processes.²⁴ Furthermore, the presence of conductive, elastic carbon also plays a positive role to improve the electrochemical performance of MoS₂–C electrodes by lowering the internal electrode resistance and effectively buffering the structural variation upon lithium uptake and removal. As a result of enhanced structural stability and diffusion kinetics, the electrochemical performance, especially the long-term capacity retention, of the MoS₂–C materials is reasonably improved.

CONCLUSIONS

In summary, we have successfully demonstrated a facile approach for the mass production of MoS₂–C 1D nanostructures by sulfidation of MoO_x/PANI nanotubes or nanowires with H₂S gas at a relative low temperature. In favor of the unique structural features, these MoS₂–C hybrid structures exhibit significantly improved electrochemical performance while evaluated as the anode materials for lithium-ion batteries. Encouragingly, the MoS₂–C nanotubes can deliver a high capacity of 776 mA h g⁻¹ after 100 cycles at a current density of 200 mA g⁻¹ and greatly improved high-rate capability at 1000 mA g⁻¹. Considering the facile fabrication method and remarkably improved electrochemical performance, these MoS₂–C hybrid materials should be of interest for constructing high-energy lithium-ion batteries.

AUTHOR INFORMATION

Corresponding Author

*E-mail: zguo@uow.edu.au (Z.P.G.); xwlou@ntu.edu.sg (X.W.L.).

Notes

The authors declare no competing financial interest.

ACKNOWLEDGMENTS

Z.P.G. acknowledges the financial support from Australian Research Council through a Discovery Project (DP1094261).

REFERENCES

- (1) Armand, M.; Tarascon, J. M. *Nature* **2008**, *451*, 652–657.
- (2) Bruce, P. G.; Freunberger, S. A.; Hardwick, L. J.; Tarascon, J.-M. *Nat. Mater.* **2012**, *11*, 19–29.
- (3) Han, Y.; Wang, Y. P.; Gao, W. H.; Wang, Y. J.; Jiao, L. F.; Yuan, H. T.; Liu, S. X. *Powder Technol.* **2011**, *212*, 64–68.
- (4) Luo, B.; Fang, Y.; Wang, B.; Zhou, J. S.; Song, H. H.; Zhi, L. J. *Energy Environ. Sci.* **2012**, *5*, 5226–5230.
- (5) Feng, C. Q.; Huang, L. F.; Guo, Z. P.; Liu, H. K. *Electrochim. Commun.* **2007**, *9*, 119–122.
- (6) Zhang, D.; Tu, J. P.; Xiang, J. Y.; Qiao, Y. Q.; Xia, X. H.; Wang, X. L.; Gu, C. D. *Electrochim. Acta* **2011**, *56*, 9980–9985.
- (7) Ding, S.; Zhang, D.; Chen, J. S.; Lou, X. W. *Nanoscale* **2012**, *4*, 95–98.
- (8) Wang, Q. H.; Jiao, L. F.; Han, Y.; Du, H. M.; Peng, W. X.; Huan, Q. N.; Song, D. W.; Si, Y. C.; Wang, Y. J.; Yuan, H. T. *J. Phys. Chem. C* **2011**, *115*, 8300–8304.
- (9) Xiao, J.; Wang, X. J.; Yang, X. Q.; Xun, S. D.; Liu, G.; Koech, P. K.; Liu, J.; Lemmon, J. P. *Adv. Funct. Mater.* **2011**, *21*, 2840–2846.
- (10) Liu, H.; Su, D.; Zhou, R.; Sun, B.; Wang, G.; Qiao, S. Z. *Adv. Energy Mater.* **2012**, DOI: 10.1002/aenm.201200087.
- (11) Chang, K.; Chen, W. X. *ACS Nano* **2011**, *5*, 4720–4728.
- (12) Du, G. D.; Guo, Z. P.; Wang, S. Q.; Zeng, R.; Chen, Z. X.; Liu, H. K. *Chem. Commun.* **2010**, *46*, 1106–1108.
- (13) Chang, K.; Chen, W. X.; Ma, L.; Li, H.; Li, H.; Huang, F. H.; Xu, Z. D.; Zhang, Q. B.; Lee, J. Y. *J. Mater. Chem.* **2011**, *21*, 6251–6257.
- (14) Chen, Z. B.; Cummins, D.; Reinecke, B. N.; Clark, E.; Sunkara, M. K.; Jaramillo, T. F. *Nano Lett.* **2011**, *11*, 4168–4175.
- (15) Ding, S. J.; Chen, J. S.; Lou, X. W. *Chem.—Eur. J.* **2011**, *17*, 13142–13145.
- (16) Feng, C. Q.; Ma, J.; Li, H.; Zeng, R.; Guo, Z. P.; Liu, H. K. *Mater. Res. Bull.* **2009**, *44*, 1811–1815.
- (17) Li, H.; Li, W.; Ma, L.; Chen, W.; Wang, J. *J. Alloys Compd.* **2009**, *471*, 442–447.
- (18) Zhang, C.; Wu, H. B.; Guo, Z.; Lou, X. W. D. *Electrochim. Commun.* **2012**, DOI: 10.1016/j.elecom.2012.1003.1039.
- (19) Wang, S. N.; Gao, Q. S.; Zhang, Y. H.; Gao, J.; Sun, X. H.; Tang, Y. *Chem.—Eur. J.* **2011**, *17*, 1465–1472.
- (20) Chang, K.; Chen, W. X. *Chem. Commun.* **2011**, *47*, 4252–4254.
- (21) Ding, Y. L.; Xie, J. A.; Cao, G. S.; Zhu, T. J.; Yu, H. M.; Zhao, X. B. *Adv. Funct. Mater.* **2011**, *21*, 348–355.
- (22) Lou, X. W.; Deng, D.; Lee, J. Y.; Feng, J.; Archer, L. A. *Adv. Mater.* **2008**, *20*, 258–262.
- (23) Wang, Z.; Su, F.; Madhavi, S.; Lou, X. W. *Nanoscale* **2011**, *3*, 1618–1623.
- (24) Wang, Z.; Luan, D.; Madhavi, S.; Hu, Y.; Lou, X. W. *Energy Environ. Sci.* **2012**, *5*, 5252–5256.